Dynamics of a wetting layer and Marangoni convection in microgravity

Ana Oprisan, John Hegseth, Gregory M. Smith, Carole Lecoutre-Chabot, Yves Garrabos, Daniel Beysens

Dynamics of a wetting layer and Marangoni convection in microgravity

Ana Oprisan[*]
Department of Physics and Astronomy, College of Charleston, Charleston, SC 29424, USA

John J. Hegseth
Department of Physics, University of New Orleans, New Orleans, LA 70148, USA

Gregory M. Smith[†]
Department of Physics and Astronomy, College of Charleston, Charleston, SC 29424, USA

Carole Lecoutre
ESEME-CNRS, Institut de Chimie de la Matière Condensée de Bordeaux, UPR 9048, Université Bordeaux I, 87 Avenue du Dr. A. Schweitzer, 33608 Pessac Cedex, France

Yves Garrabos
Institut de Chimie de la Matière Condensée de Bordeaux, UPR 9048, CNRS, 87 Avenue du Dr. Schweitzer, 33608 Pessac Cedex, France

Daniel A. Beysens
Service des Basses Températures, INAC/CEA, 17 rue des Martyrs, 38054 Grenoble Cedex 9, France ESEME, PMMH-ESPCI, 10 rue Vauquelin, 75231 Paris Cedex 5, France

(Received 22 March 2011; revised manuscript received 4 July 2011; published 22 August 2011)

Near the liquid-vapor critical point in pure fluids, material and thermal properties vary considerably with temperature. In a series of microgravity experiments, sulfur hexafluoride (SF_6) was heated ~1 K above its critical temperature, then quenched below the critical temperature in order to form gas and liquid domains. We found a power law exponent of 0.389 ± 0.010 for the growth of the wetting layer thickness during the intermediate stage of phase separation. Full and microscopic view images of the sample cell unit were analyzed to determine the changes in the size distribution of liquid droplets inside the gas phase over time. We found that the distribution of diameters for liquid droplets always contains a fraction of very small droplets, presumably due to a continuous nucleation process. At the same time, the size distribution flattens over time and rapidly includes large-size droplets, presumably generated through a coalescence mechanism. By following both a large gas bubble over two hours of video recordings, we found periodic and synchronous motion of the gas bubble along both the x and y directions. By following a large liquid droplet embedded into the large gas bubble, we found periodic, out of phase motions, which we related to Marangoni convection. The experimentally measured velocity of the liquid droplet is in good agreement with the theoretical predicted velocity of ~0.386 μm/s obtained from Young's thermocapillary effect.

DOI: 10.1103/PhysRevE.84.021202 PACS number(s): 64.75.−g, 64.70.F−, 68.03.−g, 65.20.−w

I. INTRODUCTION

During the past decades, there have been many investigations of the dynamics of phase transitions both theoretical and experimental [1]. When pure fluids in microgravity [2] or in two-component density matched mixture on Earth [3–5] are quenched from the homogeneous one-phase state through their critical point, they evolve to their final two-phase equilibrium state by the formation and growth of domains of different phases [6]. The volume fraction determines whether the system follows spinodal decomposition or a nucleation path [7,8]. The presence of solid walls and the wetting effects dramatically modify phase separation dynamics [9–14]. Both phase separation and critical wetting phenomena were studied almost independently and it was shown that these two nonequilibrium phenomena could be coupled [15]. Wetting dynamics is coupled with phase separation that takes place in the bulk of the fluid. It was shown that in the case of liquid droplet-forming phase separation, the wetting speed is much slower than in the case of bicontinuous phase separation [9].

In addition to droplet formation during phase separation, convective flows may occur. Thermocapillary migration is an important topic in material processing that is usually studied in experiments by inducing a temperature gradient inside a cell containing fluids or melted alloy [16]. Such microgravity experiments done by others showed migration of gas bubbles from low to high temperature regions due to a decrease of the interfacial tension as the temperature increases [16–19]. In the case of a gas bubble or liquid droplet, it was reported that the interfacial tension was larger at the cooler side and smaller at the warmer side. As a result, a tensile stress force will create an imbalance that pulls the surface element from the warm side to the cool side of the bubble or drop and the nearby fluid will also be pulled along leading to thermocapillary migration [20].

In this paper, we investigate the intermediate stage (IS) and late stage (LS) of the phase separation at a coexistence

[*]Corresponding author: oprisana@cofc.edu
[†]Present address: Wake Forest University, North Carolina

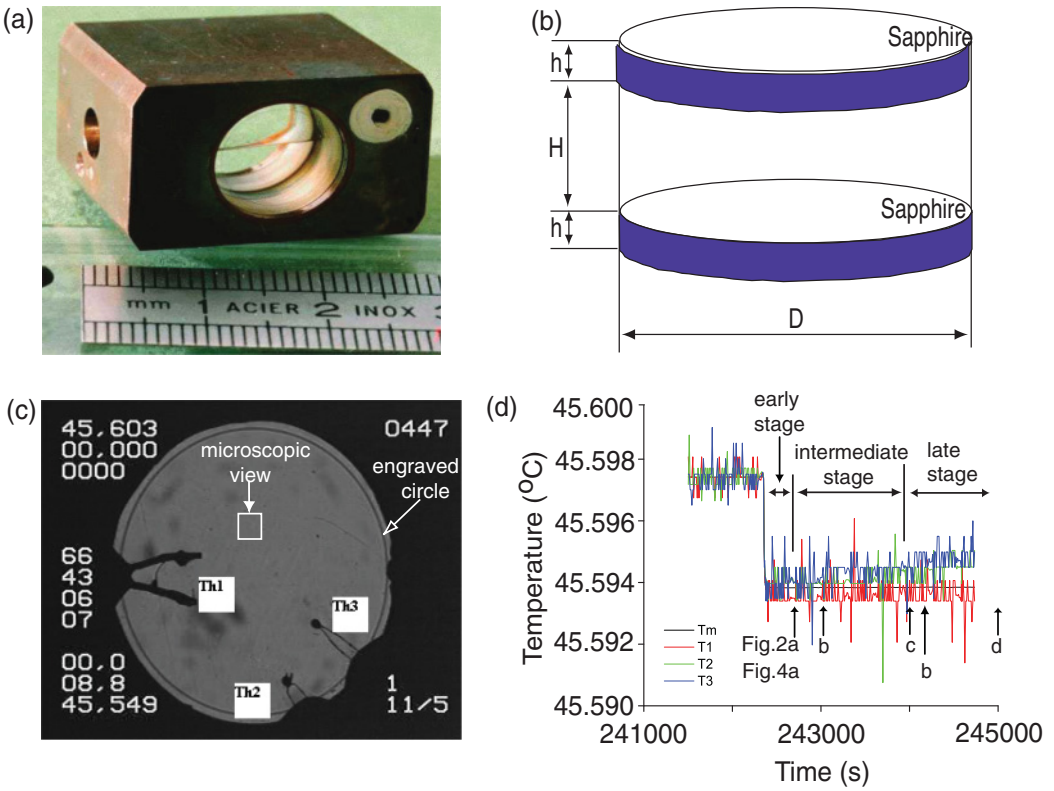

FIG. 1. (Color online) (a) The sample cell unit (SCU) used on space stations for microgravity experiments containing sulfur hexafluoride (SF_6) between two sapphire windows and a CuBeCo alloy housing. (b) A schematic representation of the SCU (not to scale) and a snapshot of a macroscopic (full) view (c) showing the locations of the three thermistors (Th_1, Th_2, Th_3) inside the SCU. The microscopic view magnifies ∼15 times the 0.9 mm × 0.9 mm square with white border placed two-thirds up from the bottom of the SCU wall along the vertical diameter. (d) Temperature profile measured by the three thermistors plus the temperature reading T_m of a thermistor embedded in the alloy housing. The early stage (ES) covers time markers between 242 399 and 242 711 s, the intermediate stage (IS) covers 242 711–243 971 s, and the late stage (LS) covers 243 971–250 000 s. The markers (a, b, c, d) in panel (d) correspond to the timing of the snapshots shown in Figs. 2 and 4, respectively.

temperature of gas and liquid phases in sulfur hexafluoride (SF_6) in microgravity and find two qualitatively different evolutions of the system. We previously showed that interconnected domains occurred during the *early stage* (ES) of phase separation (see Fig. 15 in [7]) in a supercritical pure fluid quenched through its critical point. In our experiments, the ES of phase separation starts at ∼242 389 s, measured from an arbitrary time reference that corresponds to the beginning of the microgravity experiment. The beginning of ES coincides with the moment the thermal quench was applied, and ends at ∼242 711 s, lasting ∼5 min [see Fig. 1(d)] [7]. By the end of the ES, a wetting film that separates the copper wall of the sample cell unit (SCU) and the gas bubble is clearly visible [(Fig. 2(a)].

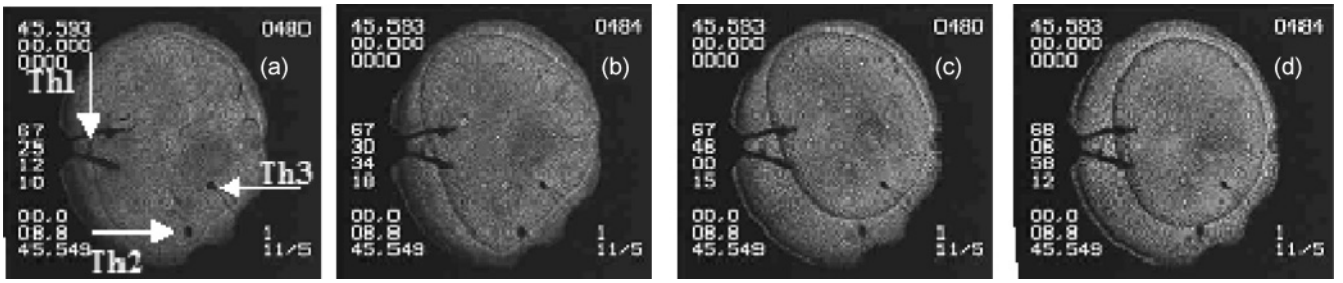

FIG. 2. Full view images showing the evolution of the wetting layer formed between the circular copper enclosure and the large gas bubble. At the crossover between the ES and the beginning of IS of phase separation (a) there is an almost homogeneous phase that separates shortly into a well-defined gas bubble insulated from the wall by a liquid layer. During the IS of phase separation (b), a large gas bubble is clearly visible and its cross section rapidly decreases. During the LS (c), (d) of phase separation, the cross section of the large gas bubble remains almost constant. Each panel corresponds to markers labeled a, b, c, d in Fig. 1(d). The corresponding time stamps for full view images are 242 712 s (a), 243 034 s (b), 244 080 s (c), and 245 338 s (d).

During the *intermediate stage* (IS) of the phase separation process that spans the time interval between 242 711 and 242 971 s, i.e., the next ∼4 min [Fig. 1(d)], the wetting layer thickness rapidly increases. *Based on our experimental data, we found a power law exponent for the growth of the average thickness of the wetting layer of 0.389 ± 0.010, with a reduced coefficient of determination of 0.997.* Our experimentally determined power law exponent of 0.389 ± 0.010 is close to the 0.30 ± 0.05 value obtained from other experiments investigating the growth of wetting layer in binary mixtures [14]. The closest theoretical prediction of a power law for the growth of wetting films belongs to Steiner and Klein [14] and is based on a diffusion-limited mechanism. As Steiner and Klein [14] mentioned when they compared their theoretical 1/4 exponent to the experimentally reported exponent of 0.30 ± 0.05, "discrepancy may reside in uncertainties [21] in the values of volume fractions and effective mobility [22] used in the coordinate reduction."

We also found that at some point during the phase separation, the wetting layer increases very slowly—a regime we call *late stage* (LS) phase separation that spans the time interval between 242 771 and 249 264 s, i.e., the next ∼108 min [Fig. 1(d)]. During the LS of the phase separation we observed thermocapillary migration in both microscopic and full view images of the SCU. The experimentally measured velocity of the largest liquid droplet embedded inside the large gas bubble (Fig. 5) was in very good agreement with the predicted value of 0.386 μm/s based on Young's theory of the thermocapillary effect. Our measurements show a periodic motion of the large gas bubble seen in the macroscopic (full) view (Fig. 7). In addition, microscopic views tracked a similar periodic motion of a much smaller liquid droplet trapped inside the large gas bubble (Fig. 5). These findings suggest that the liquid droplet trapped inside the large gas bubble undergo a thermocapillary-induced (Marangoni) convection.

II. EXPERIMENTAL SETUP

Sulfur hexafluoride (SF_6) is among the most convenient working fluids used in weightlessness to investigate critical-point phenomena. Indeed, SF_6 has a moderate critical pressure p_c (≈3.8 MPa) and critical temperature T_c (≈45.6 °C) that permit easy experimentation. In this paper, we report light transmission measurements at constant (near-critical) density that were carried out in a SF_6 sample very close to its critical point under microgravity conditions. A cylindrical cell filled with SF_6 of electronic quality, corresponding to 99.98% purity (from Alpha Gaz–Air Liquide), was placed inside of a copper cell unit [Fig. 1(a)], which in turn was placed inside a thermostat (not shown). The thermostat is specially designed for precise thermal control and aligned with the ALICE-2 optical instruments [23]. A thin layer of glue was used to seal the sapphire windows to the copper encasing and diminish the rate of heat transfer to the windows. The interior diameter of the copper cylindrical cell was $D = 12$ mm with a 10-mm circle engraved on one of the sapphire windows [Fig. 1(c)]. The thickness of each sapphire windows was $h = 9$ mm, and the thickness of the SF_6 layer was $H = 4.34$ mm [Fig. 1(b), not to scale]. This cell, whose thermal response can be estimated using a pancake cell model [24], was filled at a mean density $\langle\rho\rangle$ slightly greater than the critical density ρ_c. The relative density deviation, which is the order parameter in this experiment, $M = (\langle\rho\rangle - \rho_c)/\rho_c = 0.00 \pm 0.02\%$ was estimated on Earth using a precise optical method [25] based on the relative variation of the position of the liquid-gas meniscus, as a function of $T - T_c$ [26]. The thermistors Th_1, Th_2, Th_3 are placed inside the cell and they are all at approximately the same temperature [Fig. 1(d)]. A microscope with magnification of ∼15× was focused on a 0.9 mm × 0.9 mm area of the cell situated at two-thirds up from the bottom copper wall along the vertical diameter [white square in Fig. 1(c)]. ALICE-2 instrumentation automatically switched between macroscopic (full) views (Fig. 2) and microscopic views (Fig. 4) of the cell. The experimental data analyzed in this paper were obtained in the weightlessness of an orbiting spacecraft using ALICE-2 instrumentation, which attained high precision temperature control (stability of ≈10 μK over 50 h, repeatability of ≈40 μK over 7 d) [23,26]. The environment on board of the space station usually retains a residual gravitational acceleration, which is very low and ranges from $10^{-2}g$ (onboard aircraft in parabolic flight) to $10^{-7}g$ (onboard of Earth-orbiting research satellites), where $g = 9.8$ m/s^2 is the acceleration of gravity at the Earth's surface [27]. This residual gravity that determines the so-called microgravity environment has two components: (1) a quasisteady residual g due to aerodynamic drag, radiation pressure, micrometeorite impacts, etc.; (2) periodic residual g due to onboard machinery and natural frequencies excited by external forces. The set of numbers in the middle of the left side of Fig. 1(c) indicates the time measured from the beginning of the experiment in hours (66), minutes (43), seconds (06), and 1/25-s fractions of seconds (07), which is 240 186.28 s. We analyzed over 2 h of continuous recordings at a rate of 25 frames per second. A detailed description of the experimental setup is presented elsewhere [7].

Initially, the SCU was maintained at ∼1 K above T_c until it equilibrated to a homogeneous state. Subsequently, several sets of thermal quenches were performed from the one-phase region, above T_c, into the two-phase region, below T_c, that resulted in phase separation [7]. In this paper, we only analyzed IS and LS phase separation data from a 3.6-mK thermal quench that stepped through the critical point [Fig. 1(d)]. The temperature difference between Th_1 and Th_3 increases over time and reaches ∼1 mK [Fig. 1(d)]. The temperature difference between the two thermistors is due to the fact that Th_1 is inside the liquid layer whereas Th_3 is inside the gas bubble [Fig. 1(c)]. The reading of the measurement thermistor T_m placed inside the SCU wall represents only approximately the temperature inside the fluid phase. Density fluctuations and phase separation images were visualized through light transmission normal to the sapphire windows of the SCU using a He-Ne laser with 632.8-nm wavelength and ∼1 mW maximum power. Laser stability after 1 h was estimated to be better than 0.3% [7,26,28].

In addition to recording full view images [Fig. 1(c)], ALICE-2 instrumentation intermittently used a microscope focused on a small 0.9 mm × 0.9 mm area [white square in Fig. 1(c)]. The experimental protocol switches back and forth between macroscopic and microscopic views as follows: (1) It records full view images, (2) focuses a microscope objective

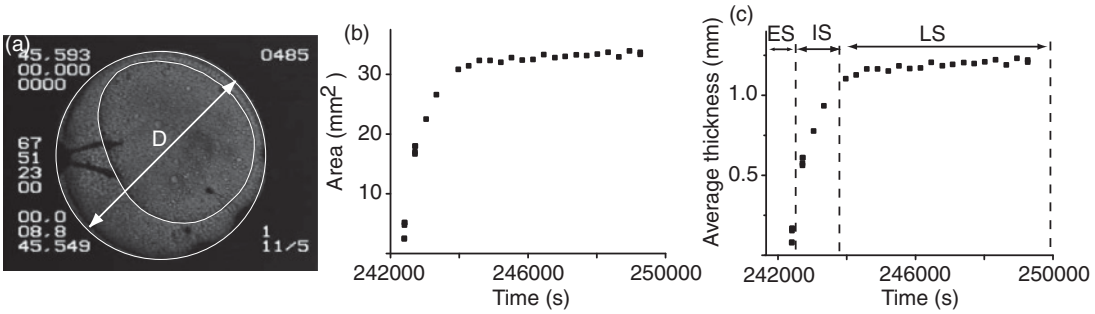

FIG. 3. (a) The wetting layer covers the area between the copper wall, marked with a white circle of diameter $D = 12$ mm, and the gas bubble is marked by a white convex and irregular contour. (b) The wetting layer area increases very quickly during the IS, between the time stamps 242 399 s and 242 721 s, and then increases very slowly during the next 108 min of the LS of phase separation. (c) The average thickness of the wetting layer fits a power law with the exponent of 0.389 ± 0.010 (with a reduced coefficient of determination of 0.997) during the fast growth of the IS of phase separation. During the LS, the power law exponent is 0.050 ± 0.006 (with a reduced coefficient of determination of 0.795).

for ∼2 s on a small 0.9 mm × 0.9 mm area and records, (3) moves the microscope objective closer to the SCU and records for another 2 s, (4) moves the microscope objective back to the initial focus plane and records for 2 s, and (5) retracts the microscope objective and records full view images of the SCU and then repeats the microscopic view recording cycle. Image analysis was carried out using ISOLUTION DT software.

III. RESULTS

We report new experimental results regarding the wetting layer dynamics following a 3.6-mK thermal quench that determined a transition from the one-phase region into the two-phase region below the critical point of SF_6 in microgravity. During the ES of the phase separation, increasingly large fluctuations of the interconnected domains were observed [7]. During the IS of phase separation, the wetting layer between the cold copper wall and the hot gas bubble grows very fast and then significantly slows down during the LS. Here we are only concerned with the IS and LS phase separation phenomena; we investigated (a) wetting layer dynamics, (b) temporal evolution of the distribution of the radii of liquid droplets inside the large gas bubble, and (3) Marangoni convection of liquid droplets coupled with the periodic motion of the large gas bubble.

A. Wetting layer dynamics from macroscopic views recorded during intermediate and late stages of phase separation

During the IS and LS of phase separation, we analyzed full view images and observed a wetting layer between the copper alloy wall and the gas bubble. We found a steady increase of the wetting layer thickness on the left side of the image where thermistor Th_1 is located [Figs. 2(a)–2(d)]. At the crossover between the ES and the beginning of the IS [Figs. 1(d) and 2(a)], the boundary of the gas-liquid interface is barely visible and the gas bubble covers almost the entire cell. The cross section of the gas bubble rapidly decreases [Figs. 1(d) and 2(b)] during the IS of the phase separation that lasts ∼4 min. During the 108 min of the LS of phase separation process [Figs. 1(d), 2(c), and 2(d)], the cross section of the gas bubble is almost constant.

We numerically estimated the area of the wetting layer by subtracting the area of the gas bubble from the cross section area of the $D = 12$ mm diameter cylindrical housing [Fig. 3(a)]. For calibration purposes, the diameter of the 10-mm circle engraved on the sapphire window was matched to ∼210 pixels, leading to a resolution of ∼48 μm/pixel in all full view images.

The off-center position of the large gas bubble (Fig. 2) was analyzed in depth by Garrabos *et al.* [29] who explained it by a small 0.46° tilt angle between the two sapphire windows. They showed that the effective acceleration that forces the gas bubble off center was $\sim 1.55 \times 10^{-3} g$, which was much larger than the $10^{-6} g$ quasistatic residual gravitational acceleration on the space station [19,29].

During the IS of the phase separation, i.e., the time stamps between 242 399 and 242 721 s, the wetting film area increases very fast, whereas it remains almost constant during the LS of phase separation, i.e., the time stamps between 242 721 and 259 264 s [Fig. 3(b)]. Based on the wetting layer area, we computed the average thickness l of the wetting layer as if it was evenly spread between two circular areas with radii $R_0 = D/2$ [Fig. 3(a)], respectively, $R_0 - l$. Since the experimentally measured wetting area is $B = A_1 - A_2$, where $A_1 = \pi {R_0}^2$ and $A_2 = \pi (R_0 - 1)^2$, the average thickness l of a uniform wetting layer is

$$l = R_0 \left(1 - \sqrt{1 - B/\pi R_0^2}\right).$$

Based on our experimental data, the power law exponent for the IS of phase separation is 0.389 ± 0.010. To our knowledge, this is the first time such an exponent was reported from experimental data obtained in weightlessness for SF_6. Our estimated power law exponent for the growth of the average thickness of the wetting layer is close to the previously reported 0.30 ± 0.05 exponent from experiments carried out on binary mixtures [14].

As far as the theoretical mechanism for wetting layer growth is concerned, Lipowsky and Huse [30] assumed nonretarded long range van der Waals interactions inside a semi-infinite wetting layer and a diffusion-limited growth mechanism for the growth of the wetting layer. They showed that the temporal evolution of the thickness of the wetting layer obeys a power law with an exponent of 1/8. Steiner and Klein [14] further

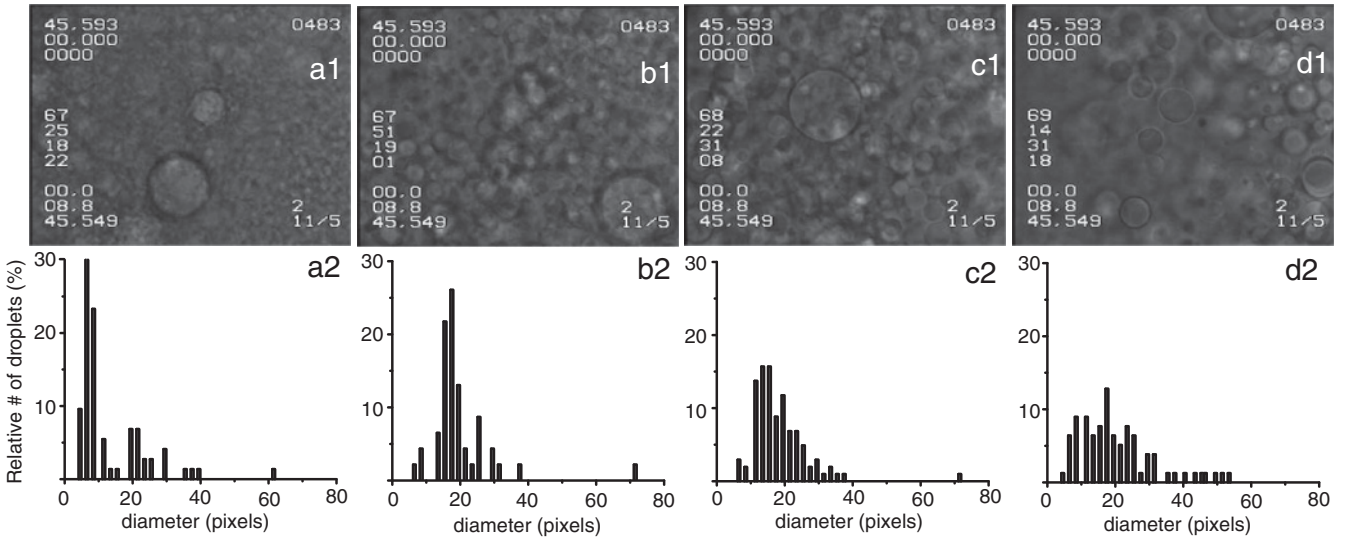

FIG. 4. Microscopic images show liquid droplets inside the large gas bubble. The microscopic view snapshots correspond to both IS with recording times of (a1) 242 718 s, and LS at (b1) 244 278 s, (c1) 246 151 s, and (d1) 249 271 s. The corresponding histograms (a2, b2, c2, and d2) show the evolution of the number and size of the liquid droplets from IS to LS of phase separation. For all microscopic view images, the resolution was $\sim$3.1 μm/pixel.

developed Lipowsky's theory by considering finite-size effects on the diffusion-limited mechanism for wetting layer growth in binary mixtures. They showed that under the new theoretical assumptions the power law exponents are actually double compared to Lipowsky's predictions. However, as Steiner and Klein [14] mentioned when comparing their theoretical 1/4 exponent to the previously reported experimental exponent of 0.30 $\pm$ 0.05, "discrepancy may reside in uncertainties [21] in the values of volume fractions and effective mobility [22] used in the coordinate reduction." As Lipowsky suggested, the formation of the thick wetting layer near the cooler copper wall is accelerated by the absence of the nucleation barriers near a solid wall for a second order wetting transition [30]. We consider that the diffusion-limited growth mechanism proposed by Lipowsky and Huse [13] and expanded by Steiner and Klein [14] is a plausible theoretical model for the experimental power law we found from our data.

B. Liquid droplet dynamics from microscopic views of the SCU during intermediate and late stage phase separation

The microscopic views were obtained by focusing a microscope on a 0.9 mm $\times$ 0.9 mm region of the full view area (Fig. 2). Based on our calibration, a 0.9-mm line in the microscopic view corresponded to 288 pixels, leading to a resolution of $\sim$3.1 μm/pixel [23,31]. We were able to measure the diameters of only a small fraction of the bulk-distributed liquid droplets comprised of only those that were close to the focus plane of the microscope (Fig. 4). The microscopic view snapshots correspond to both the IS at 242 718 s [Fig. 4(a1)], and LS at 244 278 s [Fig. 4(b1)], 246 151 s [Fig. 4(c1)], and 249 271 s [Fig. 4(d1)].

During the IS of the phase separation [Fig. 4(a1)], we found that $>$60% of the liquid droplets measured have diameters $<$8 pixels, which is $\approx$24 μm. This distribution is expected for a fluid that just emerged from large fluctuations of the interconnected domain observed during the ES of phase separation [7]. A possible explanation is that during the IS the nucleation process leads to a rapid increase in the number of small liquid bubbles [8,32–35].

After $\sim$26 min into the LS of phase separation [Fig. 1(d)], we found that $>$60% of the liquid droplets in the microscopic view have diameters between 15 and 20 pixels, i.e., 47–62 μm [Figs. 4(b1) and 4(b2)]. Such an increase in the sizes of the liquid droplets is consistent with the coalescence mechanism suggested by Beysens from other experiments

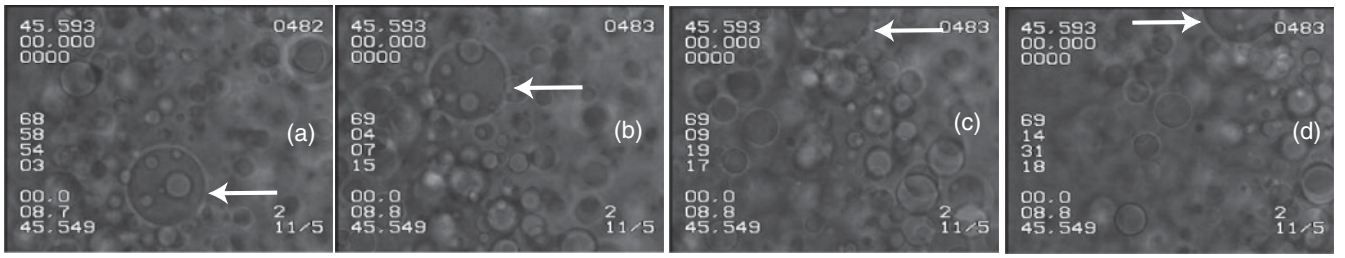

FIG. 5. Periodic motion of the 188-μm liquid droplet (indicated by the white horizontal arrow) observed during the last 25 min of the LS of phase separation in the microscopic view snapshots.

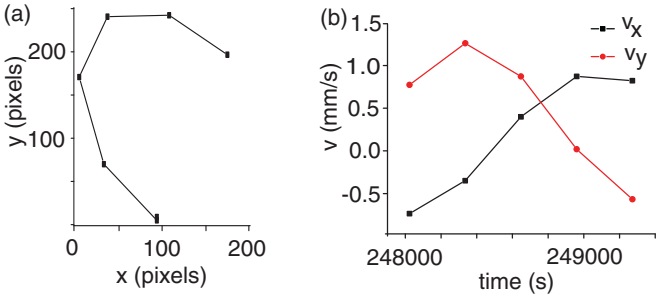

FIG. 6. (Color online) (a) The trajectory described by the center of the 188-μm liquid droplet suggests an almost circular path. (b) The corresponding velocity components of the liquid droplet.

in microgravity [6,16,36]. At the same time, the persistence of small-size liquid droplets in all distributions suggests that the nucleation process continues simultaneously with the coalescence mechanism for growth of large-size liquid droplets [37].

Towards the end of the LS of phase separation, the size distribution flattened. For example, 57 min into the LS more liquid droplets have diameters in the 15–20 pixels range, i.e., 47–62 μm [Figs. 4(c1) and 4(c2)], suggesting that small liquid droplets rapidly coalesced into larger ones [38]. The distribution of liquid droplets is almost flat in the range up to 25 pixels, which is 78 μm [Figs. 4(d1) and 4(d2)] after more than 108 min into the LS of phase separation. At the same time, we also found a significant increase in the large liquid droplets with diameters over 40 pixels, which is 124 μm [Fig. 4(d2)]. The change in the shape of the size distributions suggests that there are competing mechanisms responsible for liquid droplets growth. On one hand, small-size liquid droplets are always present in all distributions and suggests that they are continuously produced through nucleation. On the other hand, the size distribution flattens and is significantly skewed towards large-size liquid droplets during the LS, which suggests that the coalescence is presumably the mechanism driving the growth of large-size liquid droplets.

C. Marangoni convection induced by thermocapillary effects

In this section, we investigate the motion of an individual liquid droplet, which we followed throughout a series of microscopic view snapshots from 248 334 s [Fig. 5(a)], i.e., after 94 min into the LS, 248 647 s [Fig. 5(b)], 248 959 s [Fig. 5(c)], and 249 271 s [Fig. 5(d)]. It appears that the liquid droplet pointed at by the white arrow [Figs. 5(a)–5(d)] follows a circular trajectory as it changes its position in successive microscopic views ∼300 s apart. The diameter of the microscopic liquid droplet is ∼188 μm.

Since the thickness of the fluid in the SCU is over 20 times the diameter of the 188-μm liquid droplet (Fig. 5), some smaller liquid droplets appear blurred or are not visible at all in the microscopic view snapshots because they are located away from the focal plane of the microscope. It appears that four other smaller liquid droplets move in synchrony with the larger 188-μm liquid droplet [Figs. 5(a) and 5(b)], allowing us to claim that we followed the same liquid droplet in all snapshots.

We estimated the coordinates of the droplet's center and, knowing the time interval necessary to describe this motion, we estimated both the x and y components of the velocity [Fig. 6].

We also observed that the circular motion of the 188-μm liquid droplet in all microscopic view snapshots (Fig. 5) is correlated with the motion of the large gas bubble in the full view images (Fig. 2). During the last 25 min of LS recording, the large gas bubble (Fig. 7) executes a similar periodic motion like the small 188-μm liquid droplet (Fig. 5).

We measured the displacement of the large gas bubble along both the x and y directions in the cell's plane [Fig 8(a)] and computed the corresponding velocities [Fig. 8(b)]. Apart from a scaling factor that accounts for the microscope's magnification, the motion of the large gas bubble (Fig. 7) in the full view snapshots and of the 188-μm liquid droplet followed in all microscopic view snapshots (Fig. 5) correlates very well.

The large gas bubble executes a circular motion and also changes its shape while moving around due to the constraints caused by the tilt of the two sapphire windows [29]. The apparent circular motion of the large gas bubble and of the small 188-μm liquid droplet could be caused by a weak temperature gradient developing between different regions of the large gas bubble. We plotted on the same graph the vertical displacements of the liquid droplet and of the large gas bubble. Since the microscopic and macroscopic views are recorded at different times, we interpolated the large gas bubble positions to match the time stamps of the microscopic views [Fig. 9(a)]. One immediate observation is that both the large gas bubble and the small droplet inside it execute periodic motions *that are out of phase*. The explanation is as follows: The large gas bubble shrinks, as suggested by the cross section measurements (see Fig. 3). During the condensation, latent heat is released into the gas phase, which explains the higher temperature reading of the thermistor Th_3 embedded into the gas bubble with respect to the thermistor in the liquid phase. At

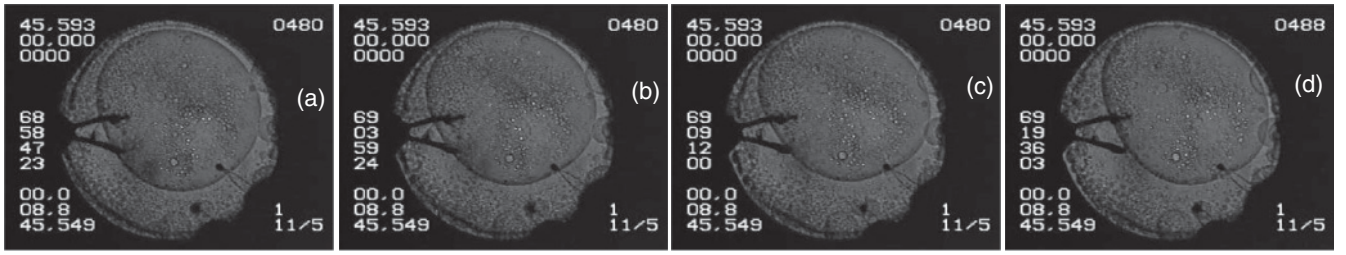

FIG. 7. Periodic motion of the large gas bubble observed during the last 25 min of phase separation.

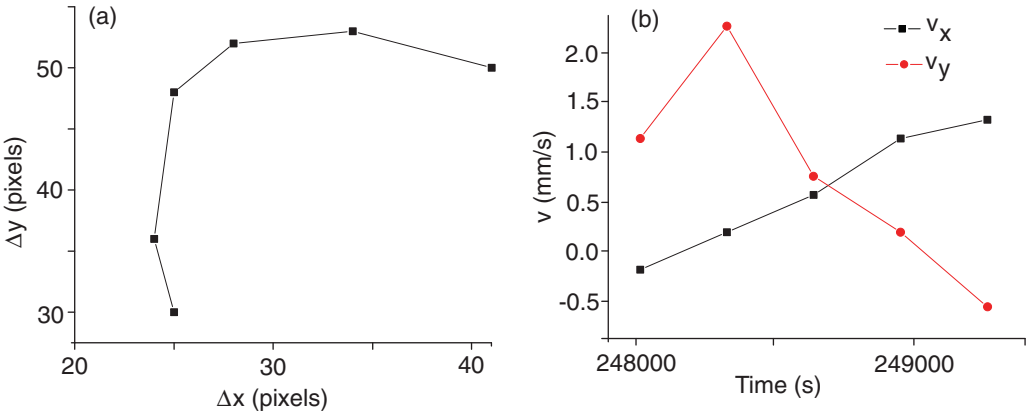

FIG. 8. (Color online) (a) The plot of the x and y displacements of the large gas bubble. (b) The estimated velocities v_x and v_y of the gas bubble.

the same time, due to fabrication imperfections, the gas bubble is not centered (see Ref. [29] for a very detailed discussion of sapphire window tilt on off-center position of the gas bubble in ALICE-2 instrumentation). As a result of the off-center position acquired by the gas bubble, the liquid layer separating the hot gas bubble from the cold copper wall varies from $\sim l_1 = 0.6$ mm at the upper right-hand corner of the SCU up to $l_2 = 3.24$ mm at the opposite side [see Fig. 9(b)]. Although near T_c the liquid phase has a very small thermal conductivity, the smaller thickness of the liquid layer at the upper right corner of the SCU dissipates latent heat from the hot gas bubble to the cold copper wall faster than the thicker liquid layer at the opposite side. Therefore, the portion of the large gas bubble closer to the cold copper wall is colder than the regions that are farther from the wall. Since the gas bubble is localized always closer to the upper right corner of the SCU, this side of the large gas bubble is the coldest and its opposite side is the hottest region of the gas bubble. This thermal gradient inside the gas bubble leads to thermocapillary convection inside the gas bubble, which we observed in all microscopic views during LS phase separation [Fig. 9(b)].

We only recorded microscopic views of the clockwise thremocapillary motion of the liquid droplets embedded in the large gas bubble due to the preset position of the microscope in ALICE-2 instrumentation [white square marking in Fig. 9(b)]. Therefore, the absence of simultaneous microscopic recordings from the lower part of the SCU to prove that there is also a counterclockwise thermocapillary motion of liquid droplets leads to the question: *How can we be sure that there is indeed a thermocapillary convection?* First, the out of phase periodic motion of the liquid droplet and the large gas bubble [Fig. 9(a)] is consistent with the conservation of momentum in Marangoni convection shown in Fig. 9(b). Specifically, while the liquid droplets near the center of the gas bubble move downward along the thermal gradient [the thick white arrow in Fig. 9(b)] the gas bubble itself moves upward to conserve the total momentum [Fig. 9(a)]. Second, the ranges of the speed of both liquid droplets and the gas bubble are similar, which is consistent both with conservation of momentum during Marangoni convection and the 50% volume fraction used for SCU preparation.

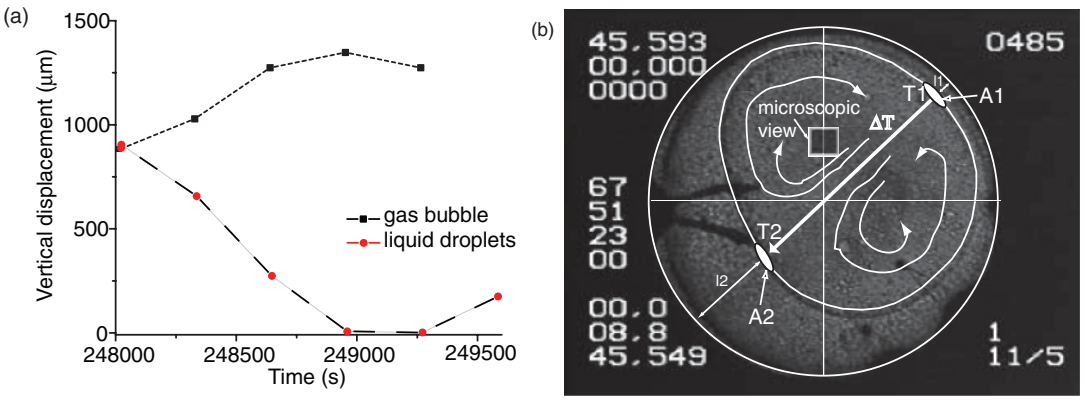

FIG. 9. (Color online) Periodic motion of the large gas bubble and the small liquid droplet inside it (a). The periodic motions of the gas bubble (dotted line) and the liquid droplet (dashed line) are out of phase. (b) Macroscopic view of the SCU (large white circle) with the gas bubble (white convex irregular shape) always hovering around the upper right corner. The heat from the hotter gas bubble dissipates faster through a thinner $l_1 = 0.6$ mm liquid layer than through the thicker $l_2 = 3.24$ mm liquid layers to the cold copper wall leading to a thermal gradient inside the large gas bubble. The liquid droplet moves clockwise in the upper half of the gas bubble due to the thermocapillary-induced convection.

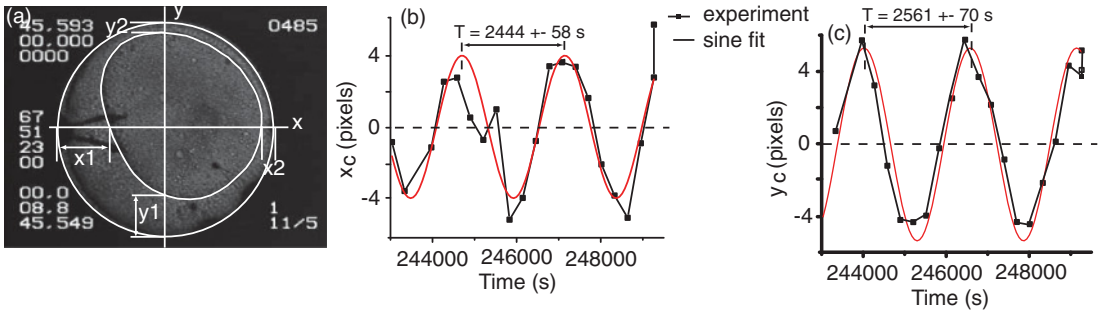

FIG. 10. (Color online) The motion of the center of the gas bubble in macroscopic view (a) provides direct evidence for an oscillatory pattern both along (b) x and (c) y directions.

To estimate the order of magnitude of the thermal gradient, we assumed that the latent heat transfer from the hot gas bubble to the cold copper wall dissipates at the same rate throughout any boundary section of the gas bubble. As a result,

$$K_{t1}A_1(T_1 - T_m)/l_1 = K_{t2}A_2(T_2 - T_m)/l_2, \qquad (1)$$

where $K_{t\,1,2}$ is thermal conductivity and $l_{1,2}$ is the thickness of the wetting layer separating the gas bubble form the copper wall, $A_{1,2}$ is the surface area, and $T_{1,2}$ is the temperature of the gas-liquid interface as marked in Fig. 9(b). Assuming equal thermal conductivity K_t around the gas bubble's contour and equal areas of the interfaces in Eq. (1), we found a temperature difference:

$$\Delta T = T_2 - T_1 = (T_2 - T_m)\,(l_2 - l_1)/l_2. \qquad (2)$$

Although we do not have measurements of the temperature T_2 at the thickest wetting layer position [Fig. 9(b)], the thermistor Th_3 is always inside the gas bubble and fortunately close enough to the desired position. Therefore, the estimated temperature difference between the upper right and the opposite side of the gas bubble is $\sim\Delta T = 1$ mK (3.24 mm–0.6 mm)/3.24 mm = 0.81 mK. The corresponding thermal gradient is

$$\Delta T/\Delta l = \Delta T/(D - l_2 - l_1) = 0.81\ \text{mK}/8.16\ \text{mm} \approx 0.1\ \text{K/m}. \qquad (3)$$

The weak temperature gradient (3) could be the source of the gradient of interfacial tension that is known to cause thermocapillary migration. Theoretical investigations of thermocapillary effect [17] predicted for the velocity of the bubbles (droplets):

$$v_{\text{th}} = \frac{2R\kappa_e}{(2\eta_e + 3\eta_i)\,(2\kappa_e + \kappa_i)}\left(\frac{\partial\gamma}{\partial T}\right)_P \nabla T, \qquad (4)$$

where v_{th} is the velocity of thermocapillary migration, R is the bubble's radius, κ is the heat conductivity, η is the dynamic viscosity, $(\frac{\partial\gamma}{\partial T})_P$ is the temperature coefficient of interfacial tension between liquid layer and gas bubble, ∇T is the weak temperature gradient between liquid layer and gas bubble, and the index e (i) refers to the gas (liquid) medium. In our case, $R = 94\ \mu$m, κ_i and κ_e were equal, η_e and η_i were equal and around 0.40×10^{-4} Kg/ms [39]. The surface tension near the critical point follows a universal law $\gamma = A(T - T_c)^n$ with $A = 51.431 \times 10^{-3}$ N/m, $T_c = 318.69$ K, $n = 1.22$ [40], which leads to $(\frac{\partial\gamma}{\partial T})_P = 9.66 \times 10^{-6}$ Kg/s^2 K. Substituting all quantities in Eq. (4) gives $v_{\text{th}} = 0.386\ \mu$m/s, which is of the same order of magnitude as our experimental value for the droplet (bubble) velocities (Fig. 6).

We also estimated the Marangoni number using the formula $Ma = \sigma_T \Delta T\, H/\nu\kappa\rho$ given by Lappa in his recent reference book [27] and the following values from similar microgravity experiment reported by Lecoutre *et al.* [26]: $\sigma_T = 9.66 \times 10^{-6}$ Kg/s^2 K; $\Delta T = 0.81$ mK; $H = 8.16$ mm; $\rho = 741$ Kg/m^3; $\nu = 0.40 \times 10^{-4}$ Kg/ms; $\kappa = 10^{-11}$ m^2/s. The estimated Marangoni number is $Ma = 215$, which is larger than the critical Marangoni number $Ma_{\text{critical}} = 100$ reported in the literature [12,41].

A periodic motion consistent with Marangoni convection was also observed in the long time scale during the entire duration of the LS of phase separation. We traced the displacement of the center of the large gas bubble in all full view snapshots taken every 1/25 s over almost 2 h of recordings (Fig. 10). The horizontal position of the center of the gas bubble can be approximated by $x_c = (x_1 - x_2)/2$ [Fig. 10(a)]. Similarly, the vertical position of the center of the gas bubble is given by $y_c = (y_1 - y_2)/2$ [Fig. 10(a)]. Both x_c [Fig. 10(b)] and y_c [Fig. 10(c)] were detrended in order to

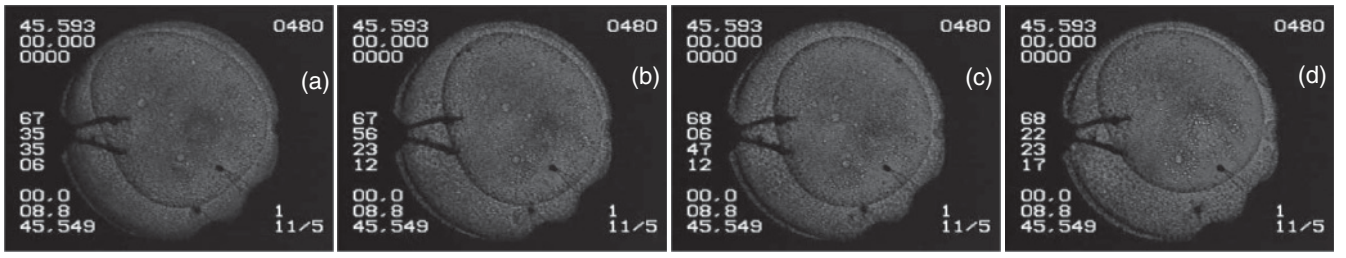

FIG. 11. Long range motion of the large gas bubble during the LS phase separation at (a) 243 335 s, (b) 244 583 s, (c) 245 207 s, and (d) 246 144 s.

emphasize the periodic motion. Our experimental results show synchronous periodic motions of the large gas bubble both in the x direction with a period $T \approx 2444$ s $\pm$ 58 s and y direction with a period of $T \approx 2561$ s $\pm$ 70 s, which correspond to a frequency in the range (3.9,4.1) 10^{-4} Hz (Fig. 10).

Such a periodic motion [Figs. 10(b) and 10(c)] can be clearly followed in successive snapshots shown in Fig. 11. After almost 10 min into the LS, the gas bubble almost touches the upper left SCU [Fig. 11(a)]. Almost 21 min later the gas bubble moved clockwise, closer to the right edge of the SCU [Fig. 11(b)]. After another 10 min the gas bubble continues its motion in the clockwise direction [Fig. 11(c)] and almost touches the top of the SCU after yet another $\sim$16 min [Fig. 11(d)].

In the study of any dynamic processes in microgravity, such as thermocapillary convection, we must always be cautious about the effect of the periodic residual g that could interfere with the actual measurements. In a recent review of all microgravity experiments carried over the last decades, Lappa [27] concluded that onboard space stations the periodic residual g was in the range from $10^{-2}g$ to $10^{-6}g$ *and* the frequency range for all observed random noises was between 0.1 and 300 Hz. In our investigation of thermocapillary effect, we found periodic motions of the gas bubble with frequencies in the range (3.9,4.1) 10^{-4} Hz. Such very low frequencies could not be explained by any chaotic g jitter. We also showed that the periodic motion of the large gas bubble is similar in both the x and y directions (Fig. 10), which is incompatible with a random g jitter. Moreover, similar experiments investigating nucleation and growth of fluid droplets in microgravity reported no correlation between the residual acceleration of gravity and the phase separation process [8].

IV. CONCLUSION

In a previous study, we investigated in detail the ES of the phase separation of SF_6 in a microgravity environment using ALICE-2 instrumentation [7]. During the ES of the phase separation, i.e., immediately after a temperature quench of 3.6 mK forced the fluid below its T_c, we observed interconnected domains growing larger and larger inside the SCU [7]. Such interconnected domains are consistent with the spinodal decomposition predicted and observed by others in microgravity at large (50%) volume fractions [5,6,23,41–44].

In this paper we report new experimental results obtained during the IS and LS of the phase separation following a 3.6-mK thermal quench in SF_6 under microgravity. During the IS of the phase separation, i.e., the next $\sim$4 min after ES, the fluctuations inside the supercritical fluid gave way to a well-defined gas bubble separated from the cold copper wall by a wetting layer. We estimated the average thickness of the wetting layer and found that it increases very quickly during the IS of the phase separation. A power law was identified for the fast growth of the average thickness of the wetting layer with an exponent of 0.389 ± 0.010 and with a reduced coefficient of determination of 0.997. Our experimental results are in good agreement with the previous exponent of 0.30 ± 0.05 from experiments carried out in binary mixtures. The theoretically predicted power law exponent by Steiner and Klein [14] is 1/4. They extended the diffusion-limited growth mechanism governed by long range van der Waals forces [45,46] proposed by Lipowsky and Huse [30] by including finite-size effects in the dynamics of the wetting layer of binary mixtures. With the caveat that the theoretical model significantly underestimates the actual power law exponent as noted by Steiner and Klein [14] ("discrepancy may reside in uncertainties [21] in the values of volume fractions and effective mobility [22] used in the coordinate reduction"), we believe that the diffusion-limited mechanism also applies to the growth of the wetting layer dynamics in pure fluids during IS. We also observed over 108 min of recordings after the IS and found that the growth of the wetting layer significantly slows down.

We also investigated the statistics of the diameter distribution for the liquid droplets in the microscopic view images during the IS and LS phase separation. We found that the peak of the distribution decreases, while the width of the distribution broadens and the position of the maximum shifts to larger diameters. The fact that the small radii liquid droplets are present in all distributions suggests that the nucleation leads to new droplet formation during both the IS and the LS phase separation. At the same time, the shape of the distribution changes by adding a long tail, which suggests that the coalescence among liquid droplets is the mechanism driving the growth of the liquid droplets.

Periodic motion of both the large gas bubble and the embedded liquid droplet was also observed during the LS of the phase separation. A possible cause is the difference in temperature between two regions of the gas bubble (see Fig. 9): the upper right region that is very close to the cold copper wall and the opposite region that is hotter. The convective flow leads to an almost periodic motion of the small liquid droplet inside the large gas bubble. At the same time, the gas bubble undergoes a periodic motion slightly out of phase with respect to the liquid droplets due to the momentum conservation. This coupled periodic motion caused by the weak temperature gradient is visible both in the full and the microscopic images. The experimentally measured velocity of the liquid droplet is in good agreement with Young's theory for thermocapillary effect [10,17,47] and numerical simulations [48–50], and it has the same order of magnitude as other experimental results [51–55]. Moreover, we found that in our experiment the Marangoni number of $Ma = 215$ was above the critical value ($Ma_{\text{critical}} = 100$) that induces thermocapillary convection. We excluded the possibility of a periodic motion of the large gas bubble and the small liquid droplets due to the randomly oriented g jitter since both x and y displacements are periodic and synchronous (Fig. 10). Moreover, prior experimental studies of phase separation in microgravity using the same or similar instrumentation did not find "any correlation between the residual accelerations and the phase separation process" [37].

ACKNOWLEDGMENTS

This work was supported by NASA Grant Nos. NAG3-1906 and NAG3-2447 to J.H., and the NASA-SCSGC grant and a Research and Development grant from the College of Charleston to A.O. We are grateful to anonymous reviewers for invaluable comments and suggestions.

[1] A. Onuki, *Phase Transition Dynamics* (Cambridge University Press, Cambridge, UK, 2002).
[2] P. Guenoun, B. Khalil, D. Beysens, Y. Garrabos, F. Kammoun, B. Le Neindre, and B. Zappoli, Phys. Rev. E **47**, 1531 (1993).
[3] C. Houessou, P. Guenoun, R. Gastaud, F. Perrot, and D. Beysens, Phys. Rev. A **32**, 1818 (1985).
[4] P. Guenoun, R. Gastaud, F. Perrot, and D. Beysens, Phys. Rev. A **36**, 4876 (1987).
[5] D. Beysens, P. Guenoun, and F. Perrot, Phys. Rev. A **38**, 4173 (1988).
[6] D. Beysens and Y. Garrabos, Physica A **281**, 361 (2000).
[7] A. Oprisan, S. A. Oprisan, J. J. Hegseth, Y. Garrabos, C. Lecoutre-Chabot, and D. Beysens, Phys. Rev. E **77**, 051118 (2008).
[8] F. Perrot, P. Guenoun, T. Baumberger, D. Beysens, Y. Garrabos, and B. Le Neindre, Phys. Rev. Lett. **73**, 688 (1994).
[9] D. Bonn, E. Bertrand, J. Meunier, and R. Blossey, Phys. Rev. Lett. **84**, 4661 (2000).
[10] D. Fenistein, D. Bonn, S. Rafai, G. H. Wegdam, J. Meunier, A. O. Parry, and M. M. Telo da Gama, Phys. Rev. Lett. **89**, 096101 (2002).
[11] P. Guenoun, D. Beysens, and M. Robert, Phys. Rev. Lett. **65**, 2406 (1990).
[12] J. Hegseth *et al.*, Int. J. Thermophys. **23**, 89 (2002).
[13] R. Lipowsky and D. A. Huse, Phys. Rev. Lett. **57**, 353 (1986).
[14] U. Steiner and J. Klein, Phys. Rev. Lett. **77**, 2526 (1996).
[15] H. Tanaka and T. Araki, Europhys. Lett. **51**, 154 (2000).
[16] D. Beysens *et al.*, Europhys. Lett. **59**, 245 (2002).
[17] N. O. Young, J. S. Goldstein, and M. J. Block, J. Fluid Mech. **6**, 350 (1959).
[18] H. Klein, G. Schmitz, and D. Woermann, Phys. Rev. A **43**, 4562 (1991).
[19] C. Ikier, H. Klein, and D. Woermann, J. Colloid Interface Sci. **184**, 693 (1996).
[20] L. G. Leal, *Advanced Transport Phenomena: Fluid Mechanics and Convective Transport Processes* (Cambridge University Press, New York, 2007).
[21] F. Scheffold *et al.*, J. Chem. Phys. **104**, 8786 (1996).
[22] A. Losch *et al.*, J. Polym. Sci., Part B: Polym. Phys. **33**, 1821 (1995).
[23] J. J. Hegseth *et al.*, in *Proceedings of the Fourth Microgravity Fluid Physics and Transport Phenomena, Cleveland, OH*, 1998.
[24] Y. Garrabos *et al.*, J. Phys. IV France **11**, 23 (2001).
[25] C. Morteau, in *Second European Symposium on Fluids in Space, Neaple, Italy*, edited by A. Viviani (Edizioni Jean Gilder Congressi, Neaple, Italy, 1996), p. 327.
[26] C. Lecoutre *et al.*, Int. J. Thermophys. **30**, 810 (2009).
[27] M. Lappa, *Thermal Convection: Patterns, Evolution and Stability* (John Wiley & Sons, Chichester, UK, 2010).
[28] J. Hegseth, A. Oprisan, Y. Garrabos *et al.*, Phys. Rev. E **72**, 031602 (2005).
[29] Y. Garrabos, C. Lecoutre-Chabot, J. Hegseth *et al.*, Phys. Rev. E **64**, 051602 (2001).
[30] R. Lipowsky and D. A. Huse, Phys. Rev. Lett. **57**, 353 (1986).
[31] J. Hegseth, A. Oprisan, Y. Garrabos, V. S. Nikolayev, C. Lecoutre-Chabot, and D. Beysens, Phys. Rev. E **72**, 031602 (2005).
[32] A. S. Abyzov and J. W. P. Schmelzer, J. Chem. Phys. **127** (2007).
[33] N. P. Balsara, C. Lin, and B. Hammouda, Phys. Rev. Lett. **77**, 3847 (1996).
[34] J. W. P. Schmelzer and J. J. Schmelzer, J. Chem. Phys. **114** (2001).
[35] J. W. P. Schmelzer, A. S. Abyzov, and J. Moller, J. Chem. Phys. **121** (2004).
[36] D. Beysens, P. Guenoun, P. Sibille, and A. Kumar, Phys. Rev. E **50**, 1299 (1994).
[37] F. Perrot, D. Beysens, Y. Garrabos, T. Fröhlich, P. Guenoun, M. Bonetti, and P. Bravais, Phys. Rev. E **59**, 3079 (1999).
[38] H. Furukawa, Adv. Phys. **34**, 703 (1985).
[39] R. A. Wilkinson, G. A. Zimmerli, H. Hao, M. R. Moldover, R. F. Berg, W. L. Johnson, R. A. Ferrell, and R. W. Gammon, Phys. Rev. E **57**, 436 (1998).
[40] E. S. Wu and W. W. Webb, Phys. Rev. A **8**, 2077 (1973).
[41] E. D. Siggia, Phys. Rev. A **20**, 595 (1979).
[42] P. Guenoun, R. Gastaud, F. Perrot, and D. Beysens, Phys. Rev. A **36**, 4876 (1987).
[43] D. Beysens, J. Straub, and D. J. Turner, in *Space, A European Perspective*, edited by H. U. Walter (Springer, Berlin, 1987), p. 221.
[44] H. Tanaka, Phys. Rev. Lett. **72**, 1702 (1994).
[45] S. Rafai, D. Bonn, E. Bertrand, J. Meunier, V. C. Weiss, and J. O. Indekeu, Phys. Rev. Lett. **92**, 245701 (2004).
[46] S. Rafai, D. Bonn, and J. Meunier, Physica A **358**, 197 (2005).
[47] A. Onuki, Phys. Rev. E **79**, 046311 (2009).
[48] J. Straub, J. Betz, and R. Marek, in *Proceedings of the VIIIth European Symposium on Materials and Fluid Sciences in Microgravity, Brussels, Belgium, 12–16 April 1992*, pp. 257–264.
[49] R. Balasubramaniam and J. E. Lavery, Numer. Heat Transfer, Part A **16**, 175 (1989).
[50] M. Ehmann, G. Wozniak, and J. Siekmann, Z. Angew. Math. Mech. **72**, 347 (1992).
[51] L. Carotenuto *et al.*, Phys. Fluids **10** (1998).
[52] Q. Kang *et al.*, Microgravity Sci. Technol. **20**, 67 (2008).
[53] R. Kozak, M. Z. Saghir, and A. Viviani, Acta Astronaut. **55**, 189 (2004).
[54] B. Braun *et al.*, J. Colloid Interface Sci. **159**, 515 (1993).
[55] P. H. Hadland *et al.*, Exp. Fluids **26**, 240 (1999).